Pergamon

Int. Comm. Heat Mass Transfer, Vol. 24, No. 4, pp. 587–596, 1997

0735-1933/97 $17.00 + .00

PII S0735-1933(97)00045-6

A THREE DIMENSIONAL INVESTIGATION OF TURBULENT FLOW AND HEAT TRANSFER AROUND SHARP 180-DEG TURNS IN TWO-PASS RIB-ROUGHENED CHANNELS

C.Y.Zhao and W.Q.Tao
School of Energy and Power Engineering
Xi'an Jiaotong University
Xi'an,Shaanxi 710049
PRC

(Communicated by B.X. Wang and S.Y. Ko)

ABSTRACT

The characteristics of the turbulent flow and heat transfer around sharp 180 deg turns in relatively short two-pass rib-roughened channels were investigated numerically for the Reynolds number varying from 1.0×10^4-9.0×10^4 by using the standard K-ε model in conjunction with the wall function method. The rib height-to-hydraulic diameter ratio (e/D) is 0.05, and the rib pitch-to-height ratio is 10. The attack angle (α) is 90 deg in inlet and outlet straight duct. In addition, there are also oblique ribs (α=45) in the turn region. To verify the numerical results, experiments for the resistance coefficient and heat/mass transfer were conducted, and reasonably good agreement between numerical and experimental results was achieved. © 1997 Elsevier Science Ltd

Introduction

In modern and advanced turbine engines, to accommodate higher turbine inlet temperatures and still maintain the metal temperatures below acceptable limit, cooling of turbine blades and vanes becomes very important. A typical cooling passage can be modeled as a two-pass rectangular channel with a pair of opposite walls with rib turbulators, as depicted in Fig.1.

A number of experimental investigations on turbulent flow in such kind of duct have been performed in the past[1-4]. However, numerical studies on this subject, especially the ones with confirmation of test results, are rather limited. Zhao and Tao[5] performed a numerical study on the laminar flow in a three-

dimensional smooth channel with a 180 degree sharp turn. To the author's knowledge, the open literature contains no information on

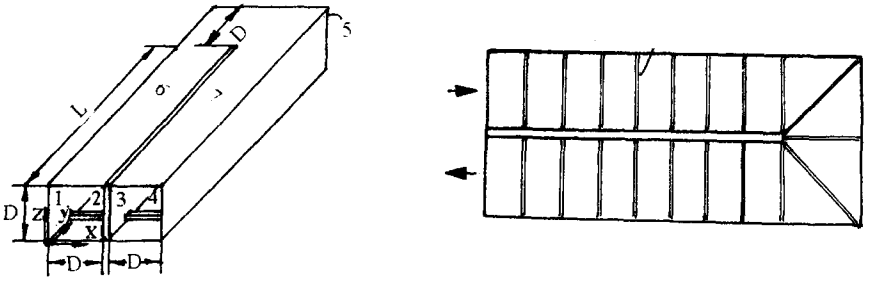

(a) Pictorial view (b) Top view

FIG.1

Configuration of the duct

the three-dimensional investigation on turbulent flow and heat transfer around sharp 180 deg turn in two-pass rib-roughened channels.

Mathematical Formulation

For turbulent flow with constant fluid properties in the rectangular channel as depicted in Fig.1. All transport equations, except for the continuity equation, can be expressed in the following general form.

$$\frac{\partial(\rho u\phi)}{\partial x}+\frac{\partial(\rho v\phi)}{\partial y}+\frac{\partial(\rho w\phi)}{\partial z}=\frac{\partial}{\partial x}(\Gamma\frac{\partial\phi}{\partial x})+\frac{\partial}{\partial y}(\Gamma\frac{\partial\phi}{\partial y})+\frac{\partial}{\partial z}(\Gamma\frac{\partial\phi}{\partial z})+S \quad (1)$$

In the above equation, ϕ is a dependent variable, such as velocity components u, v, w or temperature T.

The source term S in the above equations can be written as follows:

$$S_u=\frac{\partial}{\partial x}(\mu_t\frac{\partial u}{\partial x})+\frac{\partial}{\partial y}(\mu_t\frac{\partial v}{\partial x})+\frac{\partial}{\partial z}(\mu_t\frac{\partial w}{\partial x})-\frac{\partial p}{\partial x}$$

$$S_v=\frac{\partial}{\partial x}(\mu_t\frac{\partial u}{\partial y})+\frac{\partial}{\partial y}(\mu_t\frac{\partial v}{\partial y})+\frac{\partial}{\partial z}(\mu_t\frac{\partial w}{\partial y})-\frac{\partial p}{\partial y}$$

$$S_w=\frac{\partial}{\partial x}(\mu_t\frac{\partial u}{\partial z})+\frac{\partial}{\partial y}(\mu_t\frac{\partial v}{\partial z})+\frac{\partial}{\partial z}(\mu_t\frac{\partial w}{\partial z})-\frac{\partial p}{\partial z} \quad (2)$$

where

$$S_T=0 \qquad S_K=G-\rho\varepsilon \qquad S_\varepsilon=\frac{\varepsilon}{K}(C_1G-C_2\rho\varepsilon)$$

$$G=\mu_t\left(2\left[\left(\frac{\partial u}{\partial x}\right)^2+\left(\frac{\partial v}{\partial y}\right)^2+\left(\frac{\partial w}{\partial z}\right)^2\right]+\left(\frac{\partial u}{\partial y}+\frac{\partial v}{\partial x}\right)^2+\left(\frac{\partial u}{\partial z}+\frac{\partial w}{\partial x}\right)^2+\left(\frac{\partial v}{\partial z}+\frac{\partial w}{\partial y}\right)^2\right) \quad (3)$$

Owing to symmetry, only one-half (in Z direction) the actual duct was taken as the computational domain.

The boundary conditions are as follows:

1. At the inlet: $u_i=0$, $\bar{v}_i=Re\nu/D$, $w_i=0$, $T_i=0$

$$K_i=0.025\bar{v}_i^2 \quad (4)$$

$$\epsilon_i=100.(C_\mu\rho/Re\mu)K_i^2$$

2. At the symmetric plane of the cross-section:

$$\frac{\partial u}{\partial z}=\frac{\partial v}{\partial z}=\frac{\partial K}{\partial z}=\frac{\partial \varepsilon}{\partial z}=\frac{\partial T}{\partial z}=0 \qquad w=0 \quad (5)$$

3. At the solid surfaces, including the ones of the divider and ribs:

$$u=v=w=0 \qquad t=50°C \quad (6)$$

The wall function method was employed to deal with the wall boundary condition of K and ϵ for both the duct and rib surfaces.

4. At the duct outlet: The local one-way method[6,7] was adopted.

The governing equations were discretized by the control volume technique described in [6][7]. The iteration procedure was terminated when the relative residual of mass flow rate in the entire computation domain satisfied following condition:

$$S_{res}/M<1.0\times10^{-5} \quad (7)$$

The grid number used was 31x80x13 (in X-Y-Z). Computer source limitation prohibited us from using a finer grid system. However, from the good agreement between the numerical and experimental data of the average Nusselt number (which will be shown later), it may be considered that this is a reasonably good system.

Numerical Results and Discussion

Velocity Fields

Fig.2(a) shows the velocity field of a cross-section parallel and in close vicinity (Z/D=0.04) to the bottom surfaces for $Re=6.0\times10^4$. It can be seen that the ribs have significant effects on the flow field near the bottom surface. In the entrance section

the flow exhibits periodic character which is caused by the existence of the repeated ribs. When the bend is approached, the air flow turns inward, flowing mainly parallel to the oblique rib in the left part of the turn. Then the flow turns over the successive two ribs, forming a big recirculation in the turn region due to the combined effects of the sharp turn and the oblique ribs. In the outlet section, the flow pattern in each interval bounded by two neighboring ribs still exhibits some periodicity with an appreciable difference in flow direction. In the intervals near the duct exit, the velocity component in X-direction (i.e,u) is gradually diminished.

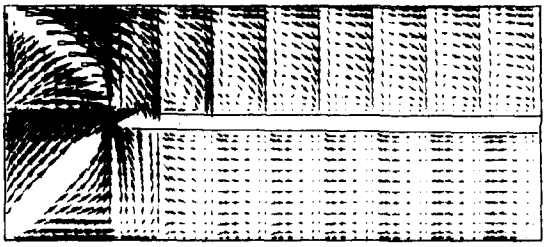

FIG.2

Predicted velocity field (XOY plane at Z/D=0.04)

Static Pressure Distribution and Resistance Coefficient

The local pressure distributions at the duct outer wall (surfaces 1,5 and 4) for $Re=6.0\times10^4$ are shown in Fig.3, where the abscissa is the dimensionless path along the mainstream direction. From the figures, we can see there is a large decrease in pressure after the turn, and the local pressure shows some fluctuation due to the effect of ribs. By comparing Fig.3(a) with Fig.3(b), it can be found that the numerically predicted pressure distribution pattern is in a good agreement with the measured results. A similar pressure distribution curve was also reported for turbulent flow in three-pass rectangular channels in the experimental work conducted by Han and Zhang[8].

In this paper, the resistance coefficient is defined as:

$$f=\frac{(\Delta P/L)D}{\rho v_i^2/2} \tag{8}$$

where L is the length along the center-line from the inlet to the outlet, over which pressure drop Δp is calculated.

The numerically predicted and experimentally measured resistance coefficients are all plotted as a function of the Reynolds number in Fig.4. It can be seen that the agreement between the numerical and experimental values is very good with a maximum deviation of about ten percent.

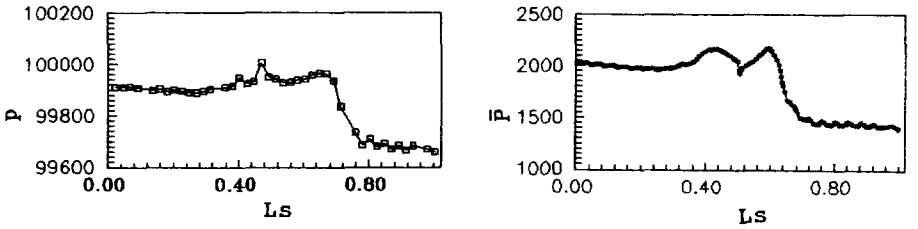

(a) Test results (b) Numerical results

FIG.3
Pressure distribution along outer wall

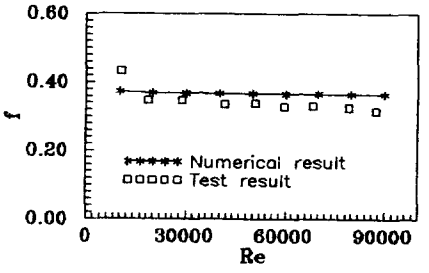

FIG.4
Resistance coefficients

Local and Average Nusselt Number

The local and surface-averaged Nusselt numbers are defined as follows:

$$Nu=\frac{\bar{h}D}{k} \qquad \overline{Nu}=\frac{\bar{h}_m D}{k} \tag{9}$$

where $\bar{h}$ is the streamwisely local heat transfer coefficient of a surface and $\bar{h}_m$ is the surface-averaged heat transfer coefficient. It should be noted that the streamwise local heat transfer coefficient $\bar{h}$ is actually an averaged value of the heightwise local heat transfer coefficients at the same streamwise location. Its numerical value is obtained by the numerical integration over the height, while its test result is the average value of two test data

measured at the centerline and the position midway between the centerline and bottom of the surface.

The distributions of the numerical and experimental streamwise local Nusselt number along the outer wall are shown in Fig.5(a) for $Re=6.0\times10^4$. From Fig.5(a), it can be seen that the numerical and experimental results have the same distribution pattern. The curves show the higher heat transfer at the channel entrance, then the rate of heat transfer drops, and it ceases changing at about the dimensionless streamwise coordinate $L_s \geq 0.2$. When the bend is approached, the Nusselt number increase abruptly, then it drops sharply, and thereafter it increases again due to the impingement, separation and reattachment of the turning flow on the outer surface. After the turn, the rate of heat transfer drops gradually. In general, the Nusselt number in after-turn is greater than that in before-turn owing to the strong effect of the turn. From Fig.5(a) we can also see that the agreement of the numerical and experimental results for the inlet and outlet duct is quite good, while in the turn region, the agreement is not so satisfactory. This is believed to be partly caused by the inherent drawback of the wall function method. Another possible reason may be attributed to the definition of the average process. For numerical one, it is the averaged value over 11 control volume, while the experimental data is the averaged value of only two local values. Because of the complexity of fluid flow in the turn region, two locations may not be enough to represent the average behavior of that streamwise location.

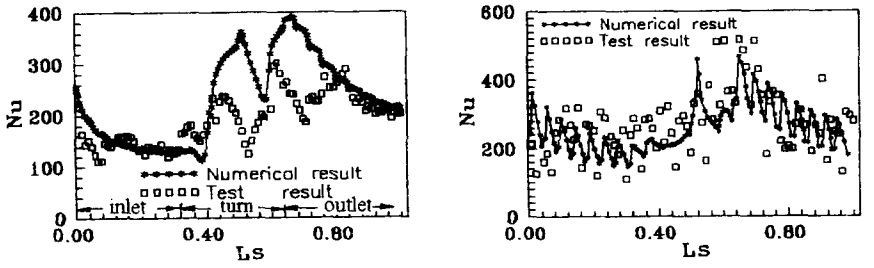

(a) Along duct outer wall (b) Along bottom wall

FIG.5

Streamwise local Nusselt number distribution

Fig.5(b) shows the numerical and experimental streamwise local Nusselt number along the bottom wall (surfaces 6 and 7). It can be

seen that the Nusselt number distribution on the bottom wall settles into a periodic pattern due to the effect of the ribs. The figures also shows that the numerical and experimental results have the same distribution trend, with the experimental results fluctuating a bit stronger than the numerical ones. For both the entrance section and the outlet section the variation of the streamwise local Nusselt number has the same trend,i.e, they decrease gradually in the streamwise direction. This is believed to be caused by the entrance effect for the former, and the strong disturbance in the turn region for the latter. Because of this strong disturbance, the level of the local Nusselt number in the outlet section is higher than that in the entrance region.

It should be noted again that the local Nusselt number discussed above is the local averaged value along the Z direction for outer wall and along the X direction for bottom wall. The actual local Nusselt number is nonuniform along the direction over which the average operation was taken. Fig.6 shows the actual local Nusselt number distributions along the different spanwise locations on bottom wall. From the figure we can see that the before-turn Nusselt number of center line is a bit greater than that of inner and outer line, and the before-turn spanwise variation is small. After the turn, the spanwise variation is much larger, and the Nusselt number of the outer line is greater than that of center line, which, in turn, is larger than that of the inner line. This is caused by the turning flow which is being forced toward the outer wall after the turn.

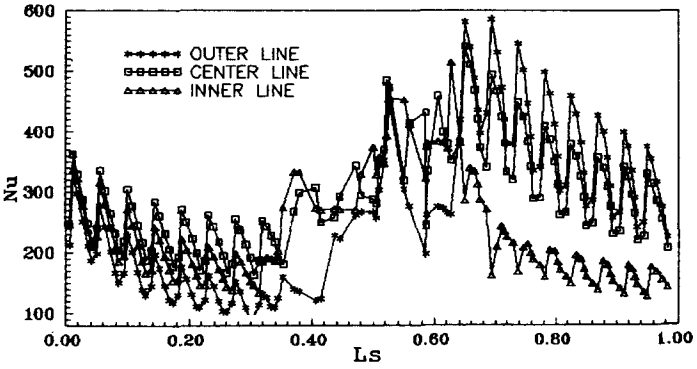

FIG.6
Actual streamwise local Nusselt number distribution

The variations of the surface-averaged Nusselt number $\overline{Nu}_m$ on each surface are plotted as a function of the Reynolds number in Figs.7(a).(b).(c).(d). From the figures we can see that the average Nusselt numbers of different surfaces all increase with the Reynolds number, and the agreement between predicted and tested Nusselt numbers for surfaces 1,2,6 and 7 is much better than that of surface 3, 4 and 5. It is to be noted that a good agreement between the predicted and measured results is obtained mainly for the surfaces consisting the entrance section(surfaces 1,2,6), while appreciable deviation occurs for the outlet section surfaces, which undergo the flow separation and reattachment caused by the bend. Thus, it is expected that the overprediction for surfaces 4 and 5, and the underprediction(surface 3) are partly caused by the imperfection of the K-ε turbulence model.

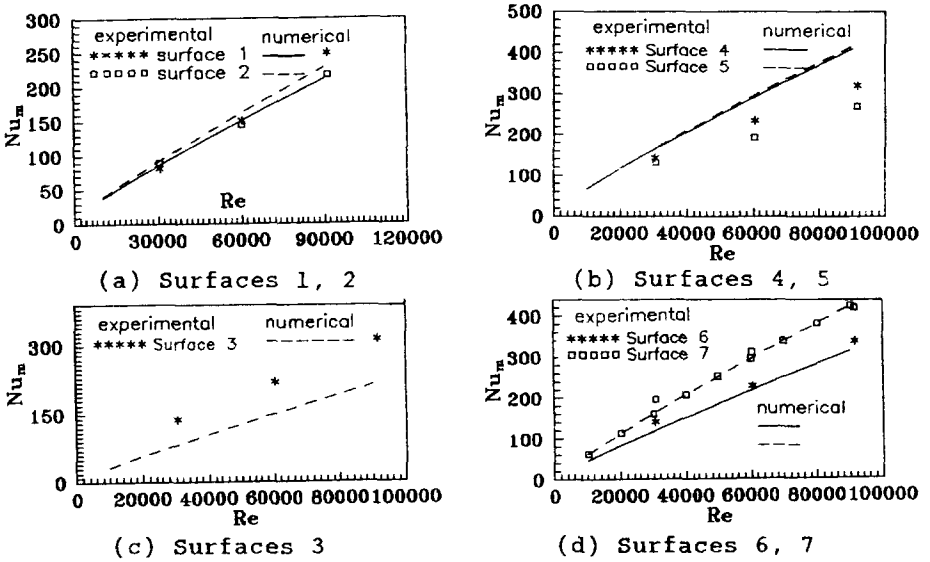

FIG.7

Surface averaged Nusselt number vs. Reynolds

Conclusions

The three-dimensional turbulent flow and heat transfer characteristics around sharp 180 deg turns in two-pass rib-roughened channels of L/D=4 have been numerically investigated by using the standard K-ε model in conjunction with the wall function method. The following conclusions can be drawn.

1. There are several recirculating zones in the turn region and

between adjacent ribs, which can not be completely discerned by a two-dimensional model.

2. The numerically predicted streamwise distribution of the local fluid pressure at the duct outer wall agrees with the experimental results quite well, and the predicted pressure distribution pattern is also consistent with the previous findings. The resistance coefficients almost remain constant for $Re=1.0\times10^4$-9.0×10^4, which have a good agreement with the experimental results.

3. The streamwise local and surface-averaged Nusselt number of the after-turn surfaces is higher than that of the before-turn surfaces. The numerical and experimental local Nusselt numbers have a similar distribution pattern, and the Nusselt numbers of bottom wall both show the periodic distributions caused by the ribs. The agreement of the inlet and outlet duct is much better than that of the turn. The agreement between the predicted and tested surface-averaged Nusselt numbers is very good for surfaces 1,2,6 and 7, while there are appreciable deviations for the surfaces 3,4 and 5, where the heat transfer behavior is largely effected by the separation and reattachment of the turning flow.

Acknowledgement

The investigation was supported by the Special Found for Doctorate of the Chinese Universities and Institutes financed by the National Educational Commission of China.

Nomenclature

C_μ	coefficient in K-ε two-equation model
D	channel width
f	resistant coefficient
G	generation term in K equation
$h,\overline{h},\overline{h}_m$	actual local, streamwisely local and surface-averaged heat transfer coefficient
k	fluid thermal conductivity
K	turbulent fluctuation kinetic energy per unit mass
L	length along the duct center-line over which Δp is determined
L_s	nondimensional streamwise coordinate based on: 1) length along the duct center-line for bottom surface 2) total length of outer surface for surfaces 1,5 and 4
M	inlet flow rate

Nu	local Nusselt number
$\overline{Nu}$	surface-averaged Nusselt number
p	pressure
$\overline{p}$	$=p-p_{ref}$, where p_{ref} is the pressure at a reference point
Pr	Prandtl number
Re	Reynolds number
S_{res}	residual of mass flow rate in entire computation domain
T	temperature
u,v,w	velocity in x,y,z directions, respectively.
$\overline{v}_i$	mean inlet velocity
x,y,z	Cartesian coordinates

Subscripts

i	inlet
t	turbulent

Greek Symbols

Γ	nominal diffusion coefficient
Δp	pressure drop across the entire duct
ϵ	dissipation rate of the turbulent kinetic energy
μ	dynamic viscosity
ρ	density

References

1. Han, J.C, Chandra, P.R, ASME Journal of Heat Transfer, 110, 91(1988).

2. Chyu, M.K, ASME Journal of Heat Transfer, 113, 63(1991)

3. Han, J.C and Zhang, P, ASME Journal of Turbomachinery, 113, 123(1991).

4. Metzger, D.E and Sahm, M.K , ASME Journal of Heat Transfer 108, 500(1984).

5. Zhao, C.Y. and Tao, W.Q., in Transport Phenomena in Thermal Fluids Engineering, Edited by Winoto,S.H, Chew, Y.T and Wijeysundera, N.E, 2, 810(1996).

6. Pantankar, S.V, Numerical Heat Transfer and Fluid Flow, Washington, D.C, New York(1980).

7. Tao, W.Q, Numerical Heat Transfer, Xi'an Jiaotong University Press, Xi'an, China(1988).

8. Han, J.C and Zhang, P, ASME Journal of Turbomachinery, 111, 515(1991).

Received November 25, 1996